X-ray and Raman study of the low temperature NH_4MnF_3 structure; evidence of librational motion of the NH_4^+ ion

1993 J. Phys.: Condens. Matter 5 283

(http://iopscience.iop.org/0953-8984/5/3/005)

J. Phys.: Condens. Matter 5 (1993) 283–300. Printed in the UK

X-ray and Raman study of the low temperature NH_4MnF_3 structure; evidence of librational motion of the NH_4^+ ion

M A Laguna†, M L Sanjuán†, V M Orera†, J Rubín†, E Palacios†, M C Piqué†, J Bartolomé†and J F Berar‡

† Instituto de Ciencia de Materiales de Aragón, CSIC-Universidad de Zaragoza, 50 009 Zaragoza, Spain

‡ Laboratoire de Chimie-Physique du Solide (UA 453 CNRS), Ecole Central, 92 295 Chatenay-Malabry Cédex, France

Received 16 July 1992, in final form 19 October 1992

Abstract. The structure of the low temperature phase of NH_4MnF_3 has been determined by means of x-ray powder diffraction using the Rietveld method. The structure is orthorhombic with space group $Pnma$, $Z = 4$. The unit cell dimensions at $T = 83$ K are $a = 5.952(1)$ Å, $b = 8.541(1)$ Å and $c = 5.949(1)$ Å. The low temperature Raman spectra have been interpreted consistently with the space group. The librational modes of the ammonium ion have been identified from the temperature dependence of the Raman lines. A model for the orientations of the NH_4^+ ions is proposed such that the minimum energy is achieved when each H atom points towards one of the four nearest F atoms. The depolarization of some of the Raman peaks is tentatively explained as an effect of orientational disorder of the NH_4^+ ions in the low temperature phase.

1. Introduction

At high temperature the ammonium fluoroperovskites NH_4MF_3 (M = Mg, Zn, Co, Mn and Cd) crystallize with a cubic phase|| ($Pm3m$, SG, $Z = 1$). At low temperatures these materials undergo a first-order transition to a lower symmetry driven by small tilts of the MF_6 octahedra.

In spite of the large number of studies devoted to the structural and magnetic properties of ammonium fluoroperovskites, the actual orientations of the ammonium ions in the non-cubic phase remain unknown. This is due in part to the micro-domain (twinning) structure of the samples, which renders the interpretation of the

|| Throughout the paper we use the international notation for space groups. For the sake of completeness, we give here the equivalent Schönflies notation for the groups that appear in the text:

International notation	Schönflies notation
$Pm3m$	O_h^1
$P4/mmm$	D_{4h}^1
$P4/mbm$	D_{4h}^5
$P4bm$	C_{4v}^2
$Pnma$	D_{2h}^{16}

We take the origin at the Mn^{2+} site, to match the standard settings of the International Crystallographic Tables for the group $Pnma$.

0953-8984/93/030283+18$07.50

experimental results difficult. This point should be elucidated in order to understand the mechanism of the phase transition.

For example, the low temperature phase of NH_4MnF_3 was first described by a tetragonal $P4/mmm$, $Z = 1$, structure resulting from a stretching of the octahedra along one of the cubic axes and a contraction in the others ($a_t = 4.2080(12)$ Å, $b_t = 4.2659(14)$ Å) (Helmholdt *et al* 1980) (notice the labelling of the pseudo-tetragonal axis as b_t), but in the perovskite structure such a distortion is quite unlikely to happen since the MF_6 octahedra tend to remain very regular (except for Jahn–Teller active metal ions). In fact, the symmetry reduction is caused in most cases by the condensation of MF_6 rotational phonon modes about the cubic axes. In-phase rotation of all octahedra along the rotation axis transforms as the M_2 irreducible representation of the cubic first Brillouin Zone (BZ), while anti-phase rotations transform as R_{15}^{+} (Glazer 1975). The actual distortion of a crystal is the result of combinations of the rotations described by these irreducible representations.

In a recent paper we have re-examined (Le Bail *et al* 1990) the crystal structure of NH_4CdF_3 through the Rietveld analysis of its powder x-ray diffraction pattern, which avoids problems related with twinning. An orthorhombic structure ($Pnma$, SG, $Z = 4$) was clearly obtained for the low symmetry phase, resulting from tilts of the octahedra around the three cubic axes ($a^-b^+a^-$ in Glazer's notation).

In this paper we apply the same technique to the NH_4MnF_3 fluoroperovskite, which has a transition temperature of $T_c = 182$ K (Palacios *et al* 1986) and shows a further transition to an antiferromagnetic phase at $T_N = 75$ K (Bartolomé *et al* 1983). In contrast with the NH_4CoF_3 compound (Bartolomé *et al* 1977a), no structural transition accompanies the magnetic one (Bartolomé *et al* 1977b). We analyse the x-ray powder diffraction pattern of NH_4MnF_3 performed at low temperature, solve the low temperature crystalline phase and compare it with that of the Cd compound.

The Raman technique has been applied successfully in helping to solve the low temperature phases of some fluoroperovskites such as $RbCdF_3$, $TlCdF_3$ (Rousseau *et al* 1975), $RbCaF_3$ (Ridou *et al* 1976) and $KMnF_3$ (Lockwood and Torrie 1974). In this paper a Raman study of the lattice modes of NH_4MnF_3 single crystals is presented. For the first time, selection rules were observed below T_c, thus allowing for a quite complete interpretation of the vibrational spectrum.

The basic quest which stirred up this work was to determine the orientations of the ammonium ion in the fluorine cage for the different phases. This point is essential in the understanding of the dynamics of the ammonium ion and its contribution to the phase transition disorder entropy (Bartolomé *et al* 1977a, Bartolomé *et al* 1983).

Most of the experimental evidence based on the study of the ammonium internal modes points towards a D_{2d} effective symmetry for the NH_4^+ ion in the cubic phase and C_s in the orthorhombic phase, with a clear indication of the existence of N–H...F bonds (Agulló-Rueda *et al* 1988, Knop *et al* 1981). However, a different model in which the N–H bonds are along the cube diagonals in the cubic phase has been proposed recently based on interatomic interaction energy calculations (Fayos 1990). To elucidate this question we also present a study of the Raman peaks corresponding to the ammonium librations and their evolution across the phase transition. The results are discussed on the basis of a possible model for ammonium orientational disorder.

2. Experimental details

Crystalline powders of NH_4MnF_3 were prepared by the reaction of $MnBr_2$ with NH_4F in methanol (Haendler *et al* 1958). NH_4MnF_3 single crystals were grown by hydrothermal synthesis, in which a stoichiometric mixture of NH_4HF and MnF_2 was heated to 673 K for one week under autogenous pressure. The crystals were small transparent cubes with dimensions of about 0.5 mm.

The x-ray powder diffraction patterns were measured at different temperatures above and below the phase transition on a two-circle powder diffractometer, using the monochromatized Cu-Kα radiation generated by a rotating anode. The scattering angle was measured with an accuracy of 0.001°, the step of the scan was 0.04° and the time per step was 10 s. The temperature stability was better than ±1 K. The analysis of the diffraction pattern was made using the Rietveld method, as adapted for x-ray powder patterns with pseudo-Voigt profiles (Bérar *et al* 1980).

The Raman spectra were measured at temperatures between 6 and 300 K in backscattering geometry, in a Dilor XY spectrometer with diode array multichannel detector. Low temperature measurements were performed in a SMC-TBT cryostat with a temperature stability of ±0.5 K. We used the 5145 Å light of a Coherent Ar^+ laser. The typical power at the sample was of the order of 50 mW. The spectral linewidth was typically better than 5 cm^{-1}.

Although great care was taken to cool down or warm up slowly, the crystals deteriorated after a few cycles, as evidenced by the formation of cracks and the loss of polarization of some Raman peaks.

3. Structure determination

The x-ray powder diffraction of NH_4MnF_3 has been measured above T_c (at 195 K) and below T_c (at 83 K) with the cryostat and at 300 K without the cryostat. The diffractogram at 195 K was fitted to the cubic $Pm3m$ structure, with a = 4.2345(1) Å, in good agreement with previous determinations at that temperature (Helmholdt *et al* 1980). This measurement and the comparison with the diffractogram at 300 K allowed us to detect a number of weak reflections which were identified as due to small amounts of impurities, or caused by the Al sample holder. These spurious peaks were included as additional peaks in the fits of the low temperature pattern.

In the diffractogram measured at 83 K the main reflections of the cubic phase were split and new reflections of small intensity corresponding to a superstructure appeared (see figure 1). As was done previously (Helmholdt *et al* 1980), the split reflections could be indexed considering an elongated tetragonal structure with a_t = 4.218 Å and b_t = 4.275 Å.

However, the superstructure peaks needed a finer analysis, which was pursued following the method proposed by Glazer (1975). First, all the main and superstructure peaks were indexed in terms of an auxiliary pseudo-tetragonal cell of $2a_t \times 2b_t \times 2c_t$ dimensions (from now on we shall take b_t = 4.275 Å as the long tetragonal axis, to compatibilize the Glazer method with the international notation). The superstructure reflections indexed as (301), (321), (341) and (325), (odd.even.odd) with $h \neq l$, imply that they are caused by small in-phase tilts of the regular MF_6 octahedra around the b_t axis, and the reflections (131) with $h = l$ and

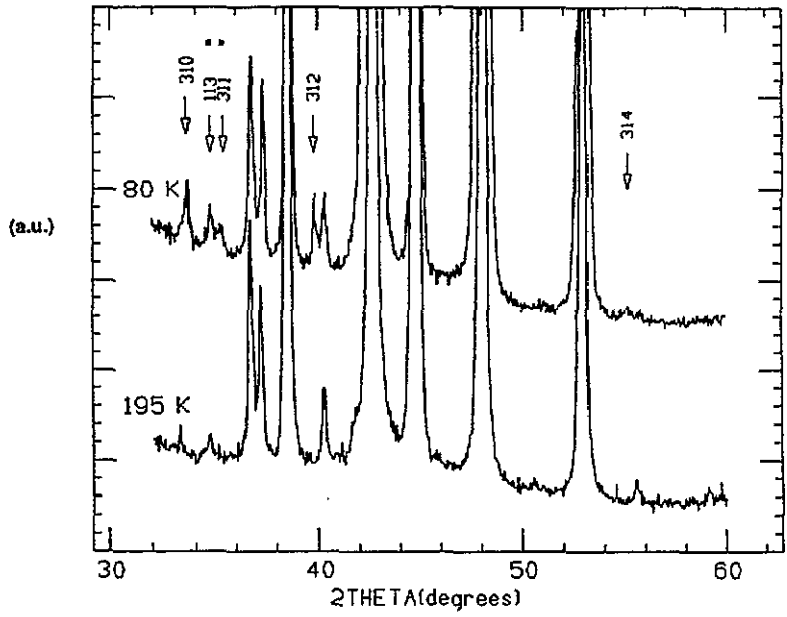

Figure 1. X-ray diffraction patterns of NH_4MnF_3 powder above (195 K) and below (80 K) $T_c = 185$ K. These include the peaks caused by the aluminium sample holder. The arrows indicate the superstructure peaks caused by the structural transition, indexed in terms of the pseudo-tetragonal $2a_t \times 2b_t \times 2c_t$ unit cell.

(311) with $k = l$, together with the condition of $a_t = c_t < b_t$, lead in a unique way to the three-tilt scheme $a_t^- b_t^+ a_t^-$ (SG, $Pnma$, $Z = 4$). This scheme corresponds to in-phase tilts around the b_t axis and to equal anti-phase tilts around the a_t and c_t axes.

Once this selection was done, a Rietveld analysis of the whole diffractogram was performed with the orthorhombic cell parameters $a \simeq a_t\sqrt{2}$, $b = 2b_t$, and $c \simeq c_t\sqrt{2}$ with $a \simeq c$. The NH_4^+ atom was considered as a point atom N, fixed in the fitting procedure at $(\frac{1}{2}, \frac{1}{4}, 0)$ since this constraint hardly affects the goodness of the fit.

In table 1(*a*) we give the best fitting parameters. The diffractogram calculated with them is compared in figure 2 with the experimental one. In table 1(*b*) the interatomic distances to the next-neighbouring atoms are given. The resulting pseudo-cubic cell is depicted in figure 3. All the Mn–F distances are nearly equal, thus verifying the starting assumption that the octahedra remain rather regular through the structural transition. The rotation angle around the pseudo-cubic axis [0,1,0] given by the M_{2y} mode takes the value of 4.7°, while around the [1,0,0] and [0,0,1], given by R'_{15x} and R'_{15z}, they are both 2.4°. The N–F distance, which is 2.99 Å in the cubic phase, varies between 2.82 and 3.19 Å. The two nearest F atoms (4, 6 in figure 3), for which the N–F distances become smaller than in the cubic phase, together with F atoms 9 and 10, form a tetrahedral cage for the NH_4^+ ion. The F atoms 2 and 8 are at slightly shorter distances than 10, while the distances for the other six are at equal or larger distances. All these results indicate that the NH_4MnF_3 compound suffers the same structural phase transition as the NH_4CdF_3 member of the series, though the distortion is smaller.

Table 1. Crystallographic data of NH_4MnF_3 at 83 K. (*a*) Best set of the adjustable parameters. $a = 5.952(1)$ Å, $b = 8.543(1)$ Å, $c = 5.949(1)$ Å, SG $Pnma$; vol $= 293.27$ Å^3; step scan (2θ deg), 0.04; 2θ range (deg), 18–130. Reliability factors (%): $R_I = 6.49$, $R_P = 5.98$, $R_{WP} = 7.75$, $R_E = 3.9$. (*b*) Characteristic interatomic distances (Å). F1 and F2 are different site types, F_n are different positions in figure 3.

(*a*)

Atom	Position	x	y	z	T	B(Å^2)
N	4*c*	0.5[a]	0.25	0.0[a]	4	0.68(8)
Mn	4*a*	0	0	0	4	0.36(2)
F_1	8*d*	0.278(3)	0.014(3)	0.761(2)	8	0.71(5)
F_2	4*c*	0	0.25	0.019(2)	4	0.71(5)

[a] Fixed value.

(*b*)

MnF_6 octahedra	N environment	Type of F atom
2×Mn–F1:2.043(1)	N–F_1:3.06(1)	1
2×Mn–F1:2.182(1)	N–F_2:2.95(1)	1
2×Mn–F2:2.139(1)	N–F_3:3.19(1)	1
(Mn–F) = 2.121	N–F_4:2.82(1)	1
	N–F_5:3.19(1)	1
	N–F_6:2.82(1)	1
	N–F_7:3.06(1)	1
	N–F_8:2.95(1)	1
	N–F_9:2.99(1)	2
	N–F_{10}:2.99(1)	2
	N–F_{11}:2.98(1)	2
	N–F_{12}:3.09(1)	2

4. Raman spectra and interpretation

In the study of the vibrational structure of the ammonium fluoroperovskites, three types of modes will be considered. The internal vibrations of the NH_4^+ ion in NH_4MnF_3 appear at frequencies above 1000 cm^{-1} and have been studied previously (Agulló-Rueda *et al* 1988), so we will not discuss them here. The lattice and ammonium librational modes appear at energies below 500 cm^{-1}. The Raman spectra of NH_4MnF_3 single crystals in this frequency range were measured at temperatures varying from 6 to 270 K ($T_c = 182$ K). Two different scattering geometries were used, which are labelled as 'xx' and 'xy', where x and y are fixed axes parallel to the crystal cube edges.

4.1. The high temperature phase

With respect to the lattice modes and neglecting the inner structure of the ammonium ion, the site symmetries in the high temperature phase, $Pm3m$, are D_{4h} for F^- and O_h for NH_4^+ and Mn^{2+}. Since all ions are at sites with inversion symmetry, they only participate in ungerade modes at $k = 0$ ($4T_{1u} + T_{2u}$), which are Raman inactive. From them, T_{2u} is infrared (IR) inactive and one of the T_{1u} is the acoustic mode with $\omega = 0$. The TO components of the other three T_{1u} modes have been observed by IR at frequencies of 163, 250 and 390 cm^{-1} (Bartolomé *et al* 1985, Patil and Secco 1972, Dunsmuir and Lane 1972).

The Raman spectrum at temperatures above the phase transition consists of a very broad band at about 330 cm^{-1}, only seen in perpendicular configuration, that

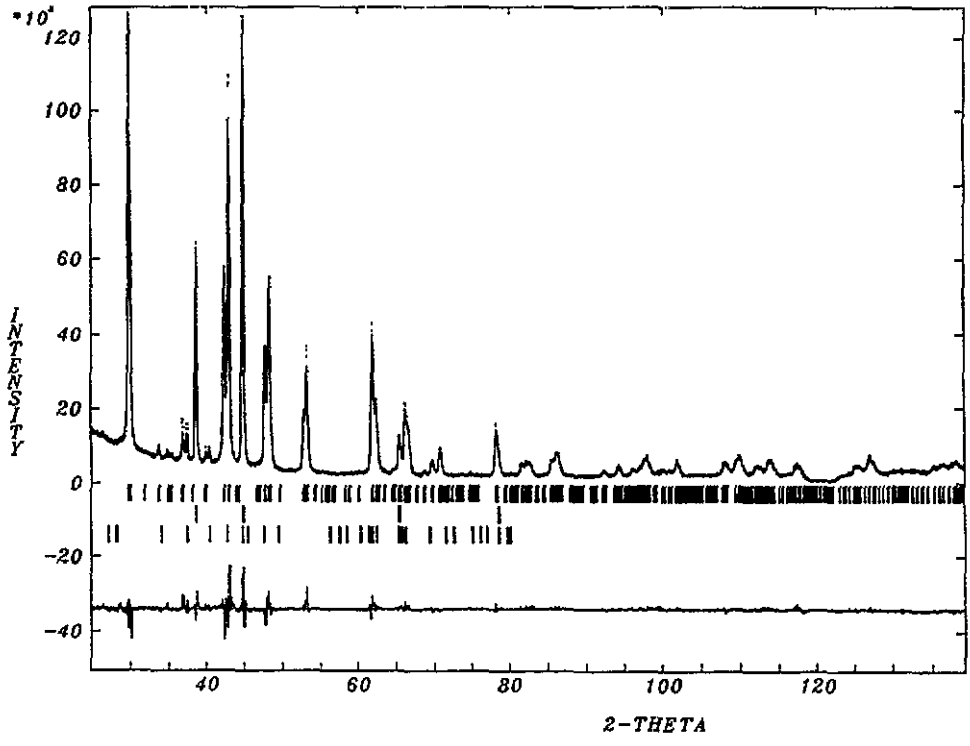

Figure 2. A comparison of the observed (dotted curve) and calculated (full curve) intensities of NH_4MnF_3. (The fit is so good that both curves are almost superposed. Dots can be seen at peak maxima. The difference pattern appears below on the same scale. The first row of vertical bars corresponds to allowed Bragg peaks, the second row to aluminium Bragg peaks, and the third row to peaks detected in the high temperature phase as impurities.

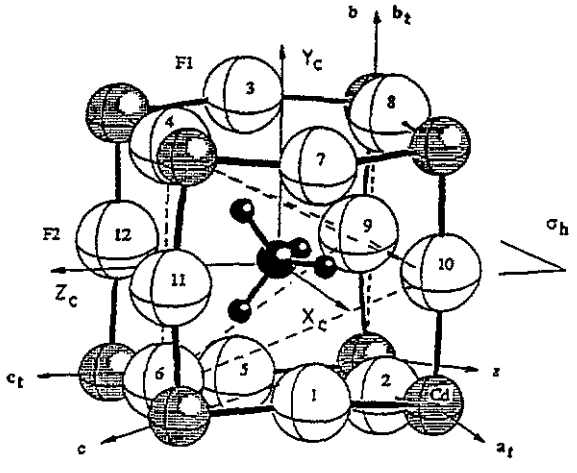

Figure 3. The surrounding atoms of the NH_4^+ ion in the $Pnma$ structure of NH_4MnF_3. The four nearest F^- ions, connected by the broken line, form a nearly tetrahedral cage of C_s symmetry. Notice the definition of the pseudo-cubic x_c, y_c and z_c axes and the σ_h plane.

has been assigned to the ammonium librations. The effective symmetry of a molecule with point group G_M located in a crystal in a site of symmetry g_i is given by $G_M \cap g_i$ or a subgroup. The point symmetry of NH_4^+ is T_d. In the cubic phase it is located in an O_h site and then its effective symmetry is $T_d \cap O_h$. When this intersection

is performed it is seen that the common elements define a D_{2d} effective symmetry if the N–H bonds are directed to fluorine ions. Ammonium librational modes in a site of such a symmetry transform as A_2 and E. Only E is Raman active and in a perpendicular configuration, as observed.

4.2. The low temperature phase

In figure 4 we show the spectra taken at 6 K in parallel and perpendicular configurations. Up to 21 Raman peaks are clearly resolved; their frequency and polarization are listed in table 2. From inspection it is obvious that some of the peaks are completely polarized in either parallel or crossed polarization, while others are only partially polarized or depolarized. The presence of well polarized peaks excludes the possibility of light depolarization due to internal stresses appearing in the cooling process.

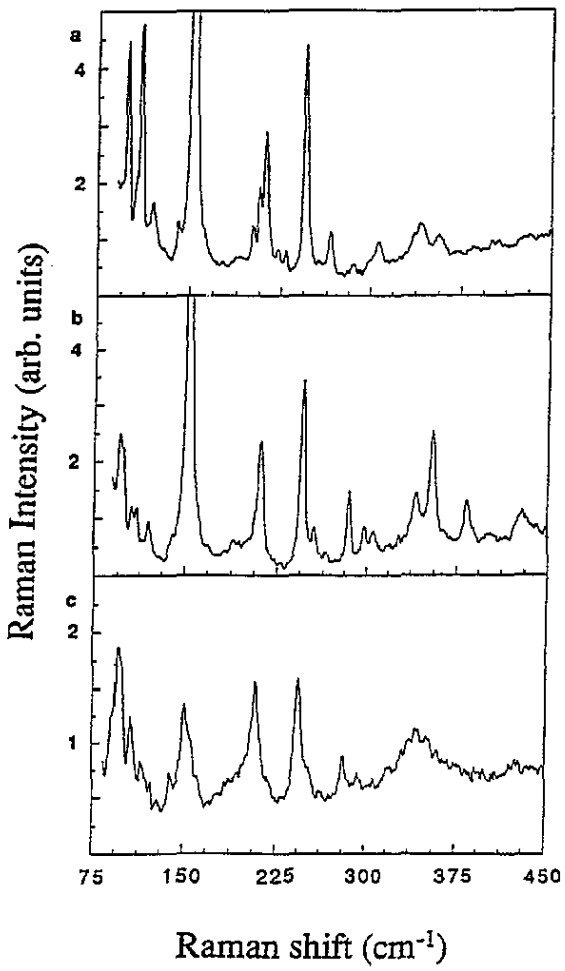

Figure 4. Low frequency Raman spectra of NH_4MnF_3 at 6 K in: (*a*), parallel (xx); (*b*), crossed (xy) polarization; and (*c*), at 160 K in crossed polarization. Notice the difference in relative intensities with the spectrum at 6 K.

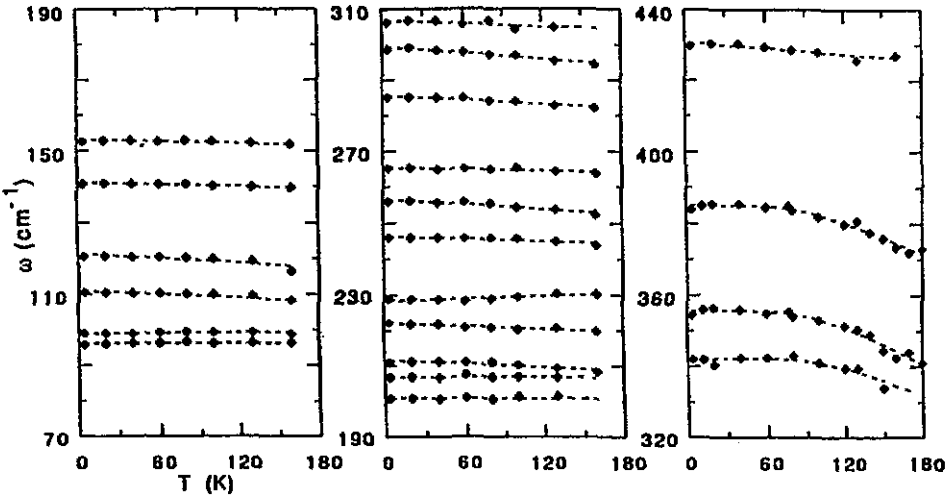

Figure 5. The temperature dependence of the low energy Raman peaks.

The temperature evolution of the Raman peak frequencies is illustrated in figure 5. We have observed neither changes on passing the magnetic transition temperature, nor evidence of the existence of soft modes. It can also be seen that the frequency decreases with temperature of the 386, 357 and 347 cm^{-1} bands are larger than in the other bands. This fact together with their coincidence in energy with the large peaks observed in inelastic neutron scattering, undoubtedly due to hydrogen motion (Rubín and Bartolomé 1992), lead us to assign these modes to ammonium librations. We will discuss this later on.

So, we are left with 18 peaks. This excludes the space group $P4/mbm$, $Z = 2$, that would give just four Raman allowed modes. Let us consider instead the orthorhombic structure $Pnma$, resulting from the condensation of the $R'_{15}(x)M_2(y)R'_{15}(z)$ mode, that has been proposed to explain the x-ray diffractogram.

Table 3. Site symmetry, lattice modes and optical activities from each site, in the low temperature phase, $Pnma$, of NH_4MnF_3.

Atom	Site	Raman active modes	IR active modes	Raman, IR inactive
$8F_{eq}$[a]	C_1	$3A_g + 3B_{1g} + 3B_{2g} + 3B_{3g}$	$3B_{1u} + 3B_{2u} + 3B_{3u}$	$3A_u$
$4NH_4$	C_s	$2A_g + B_{1g} + 2B_{2g} + B_{3g}$	$2B_{1u} + B_{2u} + 2B_{3u}$	A_u
$4F_{ax}$[b]	C_s	$2A_g + B_{1g} + 2B_{2g} + B_{3g}$	$2B_{1u} + B_{2u} + 2B_{3u}$	A_u
4Mn	C_i		$3B_{1u} + 3B_{2u} + 3B_{3u}$	$3A_u$

[a] Fluorine in σ_h plane containing Mn^{2+}.
[b] Fluorine with Mn–F bond perpendicular to σ_h.

Neglecting again the inner structure of the ammonium ion, the primitive cell of the low temperature phase contains 20 atoms, from which 60 modes are expected. The site symmetries and optical activities are given in table 3. These 60 modes at the Γ point come from the 15 modes at Γ in $Pm3m$ plus 45 modes coming from the

Table 2. Frequencies (cm^{-1}) of the Raman modes observed at 6 K in the low energy region with their polarization, symmetry assignment and correspondence with zone-edge modes of the cubic phase (in brackets: calculated frequencies in cm^{-1}). The symmetry of the librational modes is referred to the effective symmetry of the ammonium ion in each phase. The solidi indicate possible merging of bands. The plus signs indicate combination modes.

Energy (cm^{-1})	Polarization		Assignment (D_{2h}^{16})	Correlations in the cubic phase (O_h^1)
430		xy	B_{3g}	$R_1(453)$
384		xy	A''	A_2
354		xy	A''	E
342	xx	xy	A'	E
306	xx	xy	A_g	$M_3(343)$[a]
299		xy	B_{1g}	$X_1(326)$
285		xy	B_{1g}	$X_1(285)$
265	xx		B_{2g}	$M_4(254)/R'_{25}(253)$
256		xy	B_{3g}	$R'_{25}(253)$
246	xx	xy	A_g	$R'_{25}(253)$
229	xx		B_{2g}	$R'_{25}(253)/M_4(254)$
222	xx		B_{2g}	$X_5(183)$
212	xx	xy	A_g	$X_5(183)$
			B_{2g}	$R'_{25}(181)$
206	xx	xy[a]	A_g[a]	$R'_{25}(181)$[a]
201	xx		B_{2g}	$R'_{25}(181)$
153	xx	xy	A_g	$X_5(149)$
			$B_{1g} + B_{3g}$	$M_5(178)$
141	xx		B_{2g}	$X_5(149)$
121	xx	xy	A_g	$M_2(127) + R'_{15}(126)$
111	xx		B_{2g}	$R'_{15}(126)$
99	xx	xy	A_g	$R'_{15}(126) + M_2(127)$
96		xy	B_{1g}	$R'_{15}(126)$

[a] Ambiguous assignment.

BZ edge at R, M and X points. Since the 15 modes at Γ in $Pm3m$ are ungerade and ungerade modes in the cubic phase remain ungerade in the orthorhombic phase, all the allowed Raman modes (gerade) must come from the zone edge, namely, $7A_g + 5B_{1g} + 7B_{2g} + 5B_{3g}$ (24 modes, the rest up to 45 being ungerade).

4.3. Lattice modes assignment

4.3.1. Method. By standard group theory, the phonon modes of the cubic phase $Pm3m$ have been related to those of the orthorhombic phase using the group–subgroup relationship. Though there are no calculations of the dispersion relations at low temperature, we can, as an approximate step, consider the frequencies calculated for the cubic phase at M, X and R points (Bartolomé *et al* 1985) and, in view of the Raman results, propose the origin of each mode.

The calculations are based on the shell model which considers a Coulombic interaction and short-range force constants along the interatomic distances, A_i, and perpendicular to them, B_i. Using for the model parameters the values determined

from the fit to the KMF_3 compounds (Lehner *et al* 1982) and allowing the NH_4^+–F and Mn–F force constants as fit parameters†, the TO bands were fitted at room temperature. With the final set of parameters, the phonon frequencies at the BZ were calculated (Bartolomé *et al* 1985). The results for the zone boundary modes are explicitly written in table 2.

The attribution of the experimental peaks to particular modes is given in table 2 and discussed in the following paragraphs. We assume that there are no drastic changes in the force constants which describe the phonon dynamics, due to the temperature or the phase transition. Some disagreements are expected mainly due to the following causes.

(i) The values for the frequencies of the M, X and R modes were derived from the phonon dispersion curves fitted at $k = 0$ to just four high temperature IR TO modes. Consequently the extrapolation will become increasingly imprecise for k departing from zero, and most imprecise at the zone boundary.

(ii) The calculated modes in cubic symmetry will split at the structural phase transition. One may expect a shift to lower energy of those modes involving mostly translations in the 'b_t' direction, which is elongated, while motion in the a_t, c_t plane will probably result in shifts to higher frequencies.

In order to discuss the translational modes we reproduce here the Raman tensors for D_{2h} symmetry, referred to the cubic reference system:

$$\frac{1}{2}\begin{bmatrix} a+c & & -a+c \\ & 2b & \\ -a+c & & a+c \end{bmatrix}, \frac{1}{\sqrt{2}}\begin{bmatrix} & d & \\ d & & -d \\ & -d & \end{bmatrix}, \begin{bmatrix} e & & \\ & 0 & \\ & & -e \end{bmatrix}, \frac{1}{\sqrt{2}}\begin{bmatrix} & f & \\ f & & f \\ & f & \end{bmatrix}.$$

$$A_g \qquad B_{1g} \qquad B_{2g} \qquad B_{3g}$$

The structural domain structure of the sample complicates the discussion of the experimental results. There is no way of explaining our Raman results considering a single domain in either of the three possible orientations, so the assumption is taken that a homogeneous distribution of domains is present and that the local axes $\{x_l\ y_l\ z_l\}$ of a particular domain are a permutation of the $\{x\ y\ z\}$ cube axes. Then three kinds of domains are formed, having z_l parallel to x, y or z. In order to know the expected intensity of a mode in a given experimental geometry one must average the intensity arising from the three types of domains. The activities for each mode averaged for the three domains are then, in 'xx' or 'xy', the following:

	A_g	B_{1g}	B_{2g}	B_{3g}
xx	$b^2 + (a+c)^2/2$	—	$2e^2$	—
xy	$(c-a)^2/4$	d^2	—	f^2.

Then, B_{2g} modes will be seen only in xx; B_{1g} and B_{3g} only in xy, and A_g in xx and/or xy, depending on the relative values of a, b, c.

† $A_1 = 23.29$ N m^{-1}, $B_1 = -0.32$ N m^{-1}, $A_2 = 163$ N m^{-1}, $B_2 = -23.61$ N m^{-1}.

4.3.2. Assignment. The symmetry of the lattice modes can be found by means of table 2 where the data at 6 K are listed. So, the modes at 430, 299, 285, 256 and 96 cm^{-1}, appearing in xy polarization, may have B_{1g} or B_{3g} character, while those at 265, 229, 222, 201, 141 and 111 cm^{-1}, xx polarized, have B_{2g} character.

Depolarized modes are found at 246, 212, 153, 121 and 99 cm^{-1}. Some of them are, perhaps by coincidence, among the most intense. They cannot have exclusively B_{1g}, B_{2g} or B_{3g} character since these modes are fully polarized. Instead, they should be identified as A_g, which contributes both to xx and xy polarizations. The band at 206 cm^{-1} is predominantly of xx polarization; however, a shoulder is visible at that frequency on the tail of the 212 cm^{-1} peak for xy polarization.

Taking into account the above considerations, the assignment of the peaks is now performed with the aid of table 2. The mode at 430 cm^{-1} appears in xy polarization and is thus assigned to the B_{3g} coming from R_1 at 453 cm^{-1}. The modes at 384, 354 and 342 cm^{-1}, identified as ammonium librations, can mask other modes expected in this region, namely $B_{1g} + B_{3g}$ from R_{12} (342 cm^{-1}). The peak at 306 cm^{-1} is tentatively assigned to the only A_g phonon mode predicted at high frequencies, M_3 (343 cm^{-1}).

Modes at 299 cm^{-1} and 285 cm^{-1} are assigned to the two B_{1g} coming from X_1 at 326 and 285 cm^{-1}, respectively. Since these modes are near an anti-crossing point in the dispersion relations (Bartolomé *et al* 1985) their values can change significantly in the phase transition. The same can be said of the R'_{25} pair of modes. We identify the peaks at 265 and 229 cm^{-1} as B_{2g} coming either from M_4 (254 cm^{-1}) and/or from R'_{25} (253 cm^{-1}). The weak peak at 256 cm^{-1} in xy can only be the B_{3g} from R'_{25} (253 cm^{-1}). Then, the high peak at 246 cm^{-1} contains the A_g from R'_{25} (253 cm^{-1}). The B_{2g} at 222 cm^{-1} and an A_g at 212 cm^{-1} may be correlated to the split doublet X_5 (183 cm^{-1}).

The two peaks at 206 and 201 cm^{-1} are assigned to the A_g and B_{2g} components of the R'_{25} (181 cm^{-1}) triplet, respectively. The third one, of B_{3g} character, together with B_{1g} and B_{3g} coming from M_5 (178 cm^{-1}) remain unobserved; they are perhaps masked by the intense peaks at 212 cm^{-1} and/or at 153 cm^{-1}; most probably by the former, due to frequency proximity.

The strong, depolarized peak at 153 cm^{-1} and the small feature at 141 cm^{-1} are attributed tentatively to the A_g and B_{2g} components of X_5 (149 cm^{-1}), respectively. However, the strength and depolarization of the 153 cm^{-1} peak may be reflecting another effect that we shall discuss later on: the ammonium sublattice disorder. This may cause, on the one hand, selection rule breaking and depolarization, and, on the other hand, activation of formally forbidden modes. The same reason holds for other depolarized modes, such as those at 246 and 212 cm^{-1}.

We arrive finally to the 100–130 cm^{-1} region where the MnF_6 rotational modes appear. First, we assign the modes at 111 and 96 cm^{-1} to B_{2g} and B_{1g} from R'_{15} (126 cm^{-1}) (anti-phase rotation). The A_g component of this triplet, which corresponds to a combination of anti-phase rotations around a_t and c_t, couples with the A_g coming from M_2 (127 cm^{-1}, in-phase rotation around b_t) to give another pair of A_g modes, which are identified at 121 and 99 cm^{-1}. Since no softening has been observed, we cannot assign one of these two A_gs to the mode driving the phase transition.

It is important to remark that some modes with different symmetry in the cubic

phase split into modes with similar symmetry in the orthorhombic phase, which can mix to give new modes with different atomic displacements. This can explain why, in the 140 to 260 cm^{-1} region, we have some difficulty in identifying the origin of the peaks.

4.4. Librations

With respect to the librational modes, in the low temperature phase the ammonium site symmetry is C_s and the effective symmetry is also C_s. The σ_s plane is coincident with the σ_h plane of the orthorhombic lattice. Thus the allowed librational modes are $A_g + 2B_{1g} + B_{2g} + 2B_{3g} + 2A_u + B_{1u} + 2B_{2u} + B_{3u}$ when the four ammonia of the unit cell are taken into account. However, as the ammonium–ammonium coupling is expected to be very weak, many of the former librational modes will be degenerate. In fact, one may consider just the three rotational degrees of freedom of a single ammonium ion in C_s symmetry and obtain the librational modes as $2A'' + A'$, which are both Raman and IR active. Rotations around axes in the σ_s plane transform as A'' and are seen in crossed polarization (384 and 354 cm^{-1}). The rotation around the axis perpendicular to this plane (b axis) transforms as A', and is seen in crossed and parallel configurations (342 cm^{-1}).

A point charge model can be used to calculate the electrostatic potential energy of the librating NH_4^+ ion caused by the nearest-neighbour atoms. In the harmonic approximation, the diagonalization of the Schrödinger equation for rotations around the pseudo-cubic axes x_c, y_c and z_c (see figure 3) demonstrates that y_c is indeed a principal axis of libration (transforming as A'), while the two other principal axes are in the σ_s plane but rotated by 22.8° with respect to the x_c and y_c axes. In terms of an electrostatic model with interatomic distances, given in section 3, and an H effective charge of $f = 0.42e^+$ (Wagner and Hornig 1950), the calculated natural frequencies are 246 cm^{-1} for the A' mode, and 284 and 351 cm^{-1} for the two A''. So, the sequence of the splittings agrees with observation but, although the calculation helps us to assign the modes, it is far from quantitative agreement.

5. Discussion

5.1. Structures

In table 4 the available crystallographic data for the members of the $AMnF_3$ series, in the sequence of increasing unit cell size, are given for comparison purposes. From it some conclusions relevant to the NH_4MnF_3 compound may be derived.

(i) The Goldsmidt tolerance factor $t = (R_F + R_A)/\sqrt{2}(R_F + R_M)$ has been calculated for all the members of the series. One observes that if it differs from $t = 1$ by more than 4–5%, there exists a stable non-cubic phase. In the Mn fluoride series, for the Na compound $t < 1$, and the space left for the alkali ion is larger than its size. As a consequence, structural packing instability sets in, being orthorhombic at all temperatures (Ratuszna and Glazer 1988). For the K compound the instability sets in upon cooling, suffering several phase transitions (Beckman and Knox 1961, Minckiewicz *et al* 1970, Hidaka *et al* 1986). On the other hand, for the Rb and Tl compounds $t \simeq 1$, remaining cubic at all temperatures (Windsor and Stevenson 1966, Eastman and Shafer 1967). For $t > 1$ the instability sets in for the opposite reason,

Table 4. Comparison of structural transition data for the series of Mn fluoroperovskites. a, cubic cell parameter; T_c, transition temperature; t, Goldsmidt parameter; →, indicates the structural transition from the high temperature to the low temperature phase. The last column indicates the tilting of the octahedra in terms of condensed modes. For NH_4MnF_3 the t-parameter is calculated with the extreme values for the effective radius of the ammonium ion (1.675 and 1.714 Å)[g].

Compound	Ref.	a (Å)	T_c (K)	t[g]	Phases	Condensed modes
$NaMnF_3$	[a]	[3.996]†		0.894	$Pnma$	$R'_{15x} + M_{2y} + R'_{15z}$
$KMnF_3$	[b]	4.189	186	0.978	$Pm3m \rightarrow I4/mcm$	R'_{15z}
	[c]		88		$I4/mcm \rightarrow$ disorder	
			83		disorder $\rightarrow Pmmn$	$M_{2x} + M_{2y} + R'_{15z}$
$RbMnF_3$	[d]	4.2396		1.005	$Pm3m$	
NH_4MnF_3		4.242	183	0.990	$Pm3m \rightarrow Pnma$	$R'_{15x} + M_{2y} + R'_{15z}$
				1.003		
$TlMnF_3$	[e]	4.2507		0.998	$Pm3m$	
$CsMnF_3$‡	[f]	4.3308		1.058	$Pm3m$	

† a deduced from a, b and c orthorhombic parameters.
‡ High pressure phase.
[a] Ratuszna and Glazer (1988).
[b] Beckman and Knox (1961), Minckiewicz *et al* (1970).
[c] Hidaka *et al* (1986).
[d] Windsor and Stevenson (1966).
[e] Eastman and Shafer (1967).
[f] Nowotny *et al* (1970).
[g] Knop *et al* (1979).

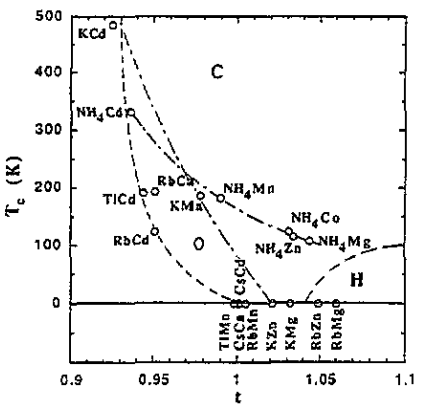

Figure 6. Variation of T_c in the fluoroperovskites with the tolerance factor t. The points are labelled with the alkali and metal-ion symbols for each AMF_3 compound. References for the data are given in table 4 and below. Guides are given for the eye, connecting common metallic-ion compounds (broken curve), and alkali compounds (chain curves). C, cubic; H, hexagonal; O, orthorhombic phases.

KCd	Darlington (1984)
TlCd, RbCd	Rousseau and Nouet (1976)
KCd, CsCd	Cousseins and Piña-Perez (1968)
RbCa	Bulou *et al* (1980)
CsCa	Rousseau *et al* (1981)
KZn	Goldsmidt and Zachariasen (1927)
RbZn	Babel (1967)
KMg	Swanson *et al* (1968)
RbMg	Shafer and McGuire (1969)

i.e. the alkali ion becomes too large for the space available. In the Cs case it is hexagonal; however, applying high pressure ($P \simeq 26$ kbar) it is possible to force the appearance of a cubic phase (Nowotny *et al* 1970).

The NH_4^+ compounds follow the same trend as the alkali-metal compounds, though some differences appear. The plot of the transition temperature, T_c, versus t (see figure 6) shows that, for a fixed divalent metal ion, as the alkali-ion radius decreases (t decreases), T_c increases. The trend is also followed by NH_4CdF_3 and

NH_4MnF_3 as members of these series. Conversely, for the same alkali ion and increasing metal-ion radius, t also decreases and T_c increases. The ammonium compounds only diverge from the trend in that there is a phase transition in all cases, irrespective of the value of t. Moreover, for a similar t its T_c is always higher than in the corresponding non-ammoniacal compound. Besides, the dependence of T_c with respect to t is less pronounced than for the other fluorides. The relative indetermination of the effective ionic radius for the NH_4^+ ion (see table 4) (Knop *et al* 1979) does not modify these conclusions.

(ii) The low temperature phase, *Pnma*, is not specific to the ammonium perovskites since it coincides with that of $NaMnF_3$, an extreme for the distorted $t < 1$ case. The Na–F distances in this compound range between 2.23 to 3.67 Å, while in NH_4MnF_3 the N–F distances just range between 2.79 and 3.2 Å. The larger difference between the extreme values for the Na compound imply that the lattice instability produces deformations much larger than the presence of the ammonium ion may induce.

(iii) For metal substitution other than Mn, the structure that appears at the same $t < 1$ extreme of the Cd series is the $KCdF_3$ compound, though in this case the K–F distances were similar to those in the ammonium counterpart. On the other hand, both NH_4MnF_3 and NH_4CdF_3 compounds distort directly to the *Pnma* structure, in contrast with other members of the series which undergo intermediate phase transitions.

From all this evidence, together with the similar analysis performed previously for Cd compounds (Le Bail *et al* 1990), one may conclude that the presence of the NH_4^+ ion in the structure does not impose a peculiar low temperature symmetry or show a significant degree of distortion. However, it enhances the stability of the low temperature phase, giving rise to a relatively higher transition temperature.

In reference to the site symmetry of the NH_4^+ ion, the observation of the E librational mode in the cubic phase excludes the model previously proposed for the ammonium orientation (Fayos 1990) in which the N–H bonds are oriented along the cube diagonals. That model would give a T_d effective symmetry that has no Raman active librational modes, contrary to observation. Conversely, our model is in agreement with the previous determination (Knop *et al* 1981) that the effective symmetry is D_{2d}, taking into account that the H atoms point toward the F ones for all different orientations.

With respect to the low temperature phase, it had been proposed for NH_4CdF_3 that the NH_4^+ ions would prefer the orientation such that the four protons point towards four F^- ions (Le Bail *et al* 1990). The same model is applicable to the Mn compound. In fact, the four N–F shorter distances in NH_4MnF_3 are nearly the same as in the Cd case. From the relative distances and librational energies determined and interpreted in terms of those distances, one may propose a model in which the two N–H...$F_{4,6}$ bonds, which are σ_s reflection related, are the strongest, the N–H...F_9 bond is intermediate, and the N–H...F_{10} bond is weakest. The NH_4^+ site is definitely of C_s symmetry.

This result solves the ambiguity of the low temperature NH_4^+ site symmetry derived from IR spectroscopy on the NH_3D^+ ion as a probe on the Mn, Zn and Co compounds (Knop *et al* 1981). It was found that the site symmetry for the NH_4^+ ion could be C_{2h} or C_s; now we know it is C_s. For the four N–H...F bonds involved in the tetrahedral cage the sequence of decreasing strength, as determined from the

shift to lower frequencies of ν_1, is in agreement with the N–H...F distance sequence of the four bonds involved in the preferential orientation.

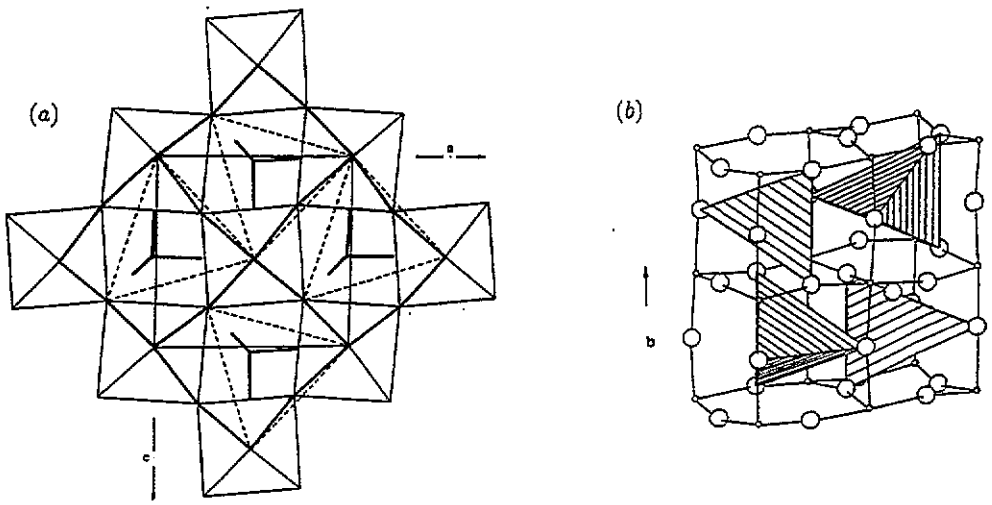

Figure 7. (*a*) View from above (*b* axis) of the first layer ($0 < z < \frac{1}{2}$) of the MF_6 octahedra and NH_4^+ ions in the $Pnma$ phase. Thin lines, orthorhombic unit cell base; thick lines, projection of four perovskite pseudo-cubes; broken lines, tetrahedral cages within each pseudo-cube. The NH_4^+ ions are shown projected onto the orthorhombic ac plane in the proposed minimum energy orientations. (*b*) Four adjoint pseudo-cubic cells showing the four different orientations of the tetrahedral cages, along the *b* axis.

In summary, the static structure below T_c consists of an ordered ammonium sublattice with a–c layers of NH_4^+ ions, such that the four nearest ones are coherently rotated by 90° around the *b* axis (see figure 7(*a*)). In adjacent layers along the *b* axis the NH_4^+ ions are rotated 180° with respect to that axis (see figure 7(*b*)).

5.2. The effect of ammonium libration and disorder

We can divide the phonon spectrum into low (< 140 cm^{-1}), intermediate (140 to 300 cm^{-1}) and high (> 300 cm^{-1}) frequency regions, corresponding to MnF_6 rotations, ammonium translations together with Mn–F bendings, and Mn–F stretchings, respectively. As the ammonium nearest neighbours are fluorine ions, ammonium translation or libration, implying N–H...F bendings, will couple strongly with F–Mn bendings. Then the modes in the intermediate frequency region will be specially sensitive to a possible disorder in the ammonium sublattice.

The space group $Pnma$ describes the symmetry of the low temperature phase only if all NH_4^+ ions are oriented in the same way with respect to their local environment; that is, if there is only one possible orientation. This is a consequence of the assumption that the orientation of the NH_4^+ ion is essentially established by the two N–H bonds which are directed towards the two nearest F ions. Since the orthorhombic distortion is such that this position is unique within each pseudo-cubic unit, no disorder can exist.

However, above T_c the ammonium ion has six equivalent orientations, and evidence of hindered rotation has been found by several techniques (Bartolomé *et al*

1977a, Palacios *et al* 1989). An anomalous entropic contribution to the heat capacity close to $R\ln 3$ is observed, which does not correspond to the six-to-one reduction in the number of orientations. This suggests that there may be a certain degree of disorder in the ammonium orientations.

Such disorder would break both the translation periodicity of the lattice and the inversion symmetry at the Mn site. This can produce two effects: first, some degree of depolarization of allowed modes and, second, activation of modes formally forbidden in the perfect lattice, i.e. ungerade modes. Both effects will probably be most important in modes involving ammonium translation, which appear precisely in the 140–250 cm^{-1} region where the intense, depolarized modes are seen. Let us consider, for instance, the 153 cm^{-1} peak. Its energy is close to the TO component of the Γ_{15} mode at 155 cm^{-1}, which splits as $B_{1u} + B_{2u} + B_{3u}$ (IR active) below T_c, and to M_5' (155 cm^{-1}) which folds as $B_{1u} + B_{3u}$ (IR active). Three peaks are observed in the low temperature IR spectrum at 155, 163 and 168 cm^{-1} (Kaal 1981), just in the region of this anomalous Raman mode. In the same manner, the peak at 212 cm^{-1} may originate from (or be affected by) IR modes observed at 210 and 220 cm^{-1}, or from IR inactive modes with similar frequency folded from the BZ edge. There are also ungerade modes (TO-Γ_{15}, for instance, at 250 cm^{-1}) which could affect the 246 cm^{-1} Raman peak. Distinguishing between either forbidden-mode activation or just mixing with odd modes, resulting in mode depolarization as the origin of the strong non-polarized peaks, is difficult and out of the scope of this work.

There is another aspect which supports the model of ammonium-disorder-induced activity: the temperature evolution of the spectra. In figure 5(*c*) we show the xy spectrum at 160 K. It can be seen that the depolarized modes at 153, 212 and 246 cm^{-1} have decreased proportionally much less than the remaining peaks. This agrees with the fact that ammonium disorder will be thermally activated. The similar evolution of the peaks at 153, 212 and 246 cm^{-1} suggests that all of them reflect the disorder effect, as we have proposed.

The origin of such disorder is subject to argument. The number of disordered ammonium ions does not need to be high, it may be of the order of a few per cent. The ions would indeed have their own different librational frequencies, but they prove to be beyond the detection limit in both optical and neutron spectroscopies. So, the disorder may arise from the orientational quenching, upon cooling, of some of the NH_4^+ ions at the transition temperature.

However, another origin may be argued; perovskites are known to form twinned domains (e.g. a $RbCaF_3$ single crystal breaks down into 50 μm wide domains, which extend along the complete crystal) (Modine *et al* 1974). The domain boundaries create a number of sites in which the symmetry for the NH_4^+ ions is different and would, thus, account for the disordered NH_4^+ subsystem. Whether disorder arises from quenching, at domain boundaries, or in some other way, cannot be established without more detailed experiments.

6. Conclusions

The structural phase transition which takes place at $T_c = 182$ K, due to coherent rotation of the MF_6 octahedra, has the effect of creating a tetrahedral cage for the NH_4^+ ion. The two N–F1 distances are actually smaller than the two N–F2. This crystallographic conclusion confirms the conjectures (Knop *et al* 1981) with respect

to hydrogen bonding in this compound: The N–H...F bond is of the single, bent, hydrogen bond type. F1 is only bonded to one H atom while F2 is shared by two H from two different NH_4^+, so, the N–H–F1 bond is expected to be stronger than the N–H–F2 one.

The tetrahedral bonding to four F atoms seems to be geometrically favourable, stabilizing the low temperature phase, i.e. providing a higher transition temperature than its homologous non-ammoniacal perovskites, as evidenced in figure 5. A comparison of the N–F distances between the Cd and the Mn compounds confirms the general proposition for ammonium compounds (Knop *et al* 1985) that, as the Goldsmidt parameter t decreases in the series there is more room for the 12-coordinated ammonium ion and, as a consequence, four N–H...F bonds will become stronger since the repulsion forces, known to exist in the NH_4MF_3 compounds (Knop *et al* 1981) will decrease. Our results show that the N–F bonds which form the tetrahedral site are shorter in the Cd compounds than in the Mn one. According to the above argument, the activation energy for NH_4^+ rotation should be higher in the Cd compound than in the Mn, as observed in QNS experiments (Rubín and Bartolomé 1992).

As regards the phase transition type, we conclude that there is no softening of a phonon mode, i.e. all the phonon frequencies vary only slightly with temperature. However, the low temperature phase is well described in terms of the condensation of a combination of modes from the Brillouin zone boundary, a description fully justified by the observation of the Raman spectrum of zone boundary modes folded into the zone centre in the low temperature phase. All this allows us to classify the structural transition as first order, with the high symmetry phase stabilized by the increase in entropy generated by the disorder of the ammonium ions.

Some of these characteristics are common to other ammonium compounds such as NH_4Cl, NH_4Br (Wang and Wright 1973) or NH_4AlF_4 (Couzi *et al* 1985) where no lattice soft phonon was detected, although the ammonium disorder depolarized phonon hard modes and a softening of the librational mode was observed. However, in the NH_4X cases T_c increased with decreasing cell size, proving that the coupling mechanism was NH_4–NH_4 octupole–octupole interaction. In contrast, the T_c of NH_4MF_3 compounds decreases with decreasing cell size, an effect associated with the perovskite structure, not to the presence of the ammonium ion. However, the presence of ammonium enhances the stability of the low temperature structure with respect to the non-ammoniacal fluoroperovskites, as we have discussed in this paper, so it plays an effective role in the transition.

Acknowledgments

This work has been supported by the MAT88-302 CICYT and the CEE ST2P-0458-C projects. The CICYT-REDESA-UNESA MIDAS 89/3797 project has financed the micro-Raman cryostat.

References

Agulló-Rueda F, Calleja J M and Bartolomé J 1988 *J. Phys. C: Solid State Phys.* **21** 1287
Babel D 1967 *Struct. Bonding* **3** 1

Bartolomé J, Burriel R, Palacio F, González D, Navarro R, Rojo J A and de Jongh L J 1983 *Physica* B **115** 190
Bartolomé J, Navarro R, González D and de Jongh L J 1977a *Physica* B **92** 23
—— 1977b *Physica* B **92** 45
Bartolomé J, Palacio F, Calleja J M, Agulló-Rueda F, Cardona M and Migoni R 1985 *J. Phys. C: Solid State Phys.* **18** 6083
Beckman O and Knox K 1961 *Phys. Rev.* **121** 376
Bérar J F, Galvarin G and Weigel D 1980 *J. Appl. Crystallogr.* **13** 201
Bulou A, Ridou C, Rousseau M and Nouet J 1980 *J. Physique* **41** 87
Cousseins J C and Piña-Pérez C 1968 *Rev. Chim. Miner.* **5** 147
Couzi M, Rocquet P and Fourquet J L 1985 *J. Physique* **46** 435
Darlington C N W 1984 *J. Phys. C: Solid State Phys.* **17** 2859
Dunsmuir J T R and Lane A P 1972 *Spectrochim. Acta* A **28** 45
Eastman D E and Shafer M W 1967 *J. Appl. Phys.* **38** 1274
Fayos J 1990 *J. Phys. Chem. Solids* **51** 177
Glazer A M 1975 *Acta Crystallogr.* A **31** 756
Goldsmidt V M and Zachariasen W 1927 *Geochem. Verteilung* VIII 147
Haendler H M, Johnson F A and Crocket D S 1958 *J. Am. Chem. Soc.* **80** 2662
Helmholdt R B, Wiegers G A and Bartolomé J 1980 *J. Phys. C: Solid State Phys.* **13** 5081
Hidaka M, Fujii H and Maeda S 1986 *Phase Transit.* **6** 101
Kaal W 1981 *Doctoraal Proefschrift* Katholieke Universiteit, Nijmegen
Knop O, Oxton A, Westerhaus W J and Falk M 1981 *J. Chem. Soc. Faraday Trans. II* **77** 309
Knop O, Oxton I and Falk M 1979 *Can. J. Chem.* **57** 404
Knop O, Westerhaus W J, Falk M and Massa W 1985 *Can. J. Chem.* **63** 3328
Le Bail A, Fourquet J L, Rubín J, Palacios E and Bartolomé J 1990 *Physica* B **162** 231
Lehner N, Rauh H, Strobel K, Geick R, Heger G, Bonillot J, Renkers B, Rosseau M and Stirling W G 1982 *J. Phys. C: Solid State Phys.* **15** 6545
Lockwood D J and Torrie B H 1974 *J. Phys. C: Solid State Phys.* **7** 2729
Minckiewicz V J, Fujii Y and Yamada Y 1970 *J. Phys. Soc. Japan* **28** 443
Modine F A, Sonder E, Unruh W P, Finch C B and Westbrook R D 1974 *Phys. Rev.* B **10** 1623
Nowotny H, Boller H and Beckman O 1970 *J. Solid State Chem.* **2** 462
Palacios E, Bartolomé J, Burriel R and Brom H 1989 *J. Phys.: Condens. Matter* **1** 1119
Palacios E, Navarro R, Burriel R, Bartolomé J and González D 1986 *J. Chem. Thermodyn.* **18** 1089
Patil K C and Secco E A 1972 *Can. J. Chem.* **50** 1529
Ratuszna A and Glazer A M 1988 *Phase Transit.* **12** 347
Ridou C, Rousseau M, Gesland J Y, Nouet J and Zarembovitch A 1976 *Ferroelectrics* **12** 199
Rousseau M, Gesland J Y, Hennion B, Heger G and Renker B 1981 *Solid State Commun.* **38** 45
Rousseau M, Gesland J Y, Julliard J, Nouet J, Zarembovitch J and Zarembovitch A 1975 *Phys. Rev.* B **12** 1579
Rousseau M and Nouet J 1976 *Acta Crystallogr.* A **32** 263
Rubín J and Bartolomé J 1991 *Spanish Scientific Research using Neutron Scattering Techniques* ed J C Gómez Sal, M Barandiarán and T Rojo (Servicio de Publicaciones, Universidad de Cantabria)
Shafer M W and McGuire T R 1969 *J. Phys. Chem. Solids* **30** 1989
Swanson H E, McMurdie H F, Morris M C and Evans E H 1968 *USNBS Monograph* vol 25 (Washington, DC: US Government Printing Office) p 6
Wagner E L and Hornig T F 1950 *J. Chem. Phys.* **18** 296
Wang C H and Wright R B 1973 *J. Chem. Phys.* **58** 2934
Windsor C G and Stevenson R W H 1966 *Proc. Phys. Soc.* **87** 501